



Cite this: *Med. Chem. Commun.*,
2018, 9, 1619

Identification of an auxiliary druggable pocket in the DNA gyrase ATPase domain using fragment probes†

Xiaojie Huang,  Junsong Guo, Qi Liu, Qiong Gu,  Jun Xu  and Huihao Zhou*

Discovery of new drug binding sites on well-established targets is of great interest as it facilitates the design of new mechanistic inhibitors to overcome the acquired drug resistance. Small chemical fragments can easily enter and bind to the cavities on the protein surface. Thus, they can be used to probe new druggable pockets in proteins. DNA gyrase plays indispensable roles in DNA replication, and both its GyrA and GyrB subunits are clinically validated antibacterial targets. New mechanistic GyrB inhibitors are urgently desired since the withdrawal of novobiocin from the market by the FDA due to its reduced efficiency and other reasons. Here, a fragment library was screened against the *E. coli* GyrB ATPase domain by combining affinity- and bioactivity-based approaches. The following X-ray crystallographic efforts were made to determine the cocrystal structures of GyrB with ten fragment hits, and three different binding modes were disclosed. Fortunately, a hydrophobic pocket which is previously unknown was identified by two fragments. Fragments that bind to this pocket were shown to inhibit the ATPase activity as well as the DNA topological transition activity of DNA gyrase *in vitro*. A set of fragment analogs were screened to explore the binding capacity of this pocket and identify the better starting fragments for lead development. Phylogenetic analysis revealed that this pocket is conserved in most Gram-negative and also many Gram-positive human pathogenic bacteria, implying a broad-spectrum antibacterial potential and a lower risk of mutation. Thus, the novel druggable pocket and the starting fragments provide a novel basis for designing new GyrB-targeting therapeutics.

Received 16th March 2018,
Accepted 3rd July 2018

DOI: 10.1039/c8md00148k

rsc.li/medchemcomm

1. Introduction

Antibiotics are among the greatest discoveries by human beings. They save millions of lives every year. However, drug resistance to the existing antibiotics has developed quickly in recent years, which has become a serious global public health problem.¹ Discovery of new antibacterial agents with novel scaffolds and mechanisms is urgently demanded.^{2,3}

DNA gyrase is an enzyme that exists in prokaryotes but not in humans. It relaxes the positive supercoil and introduces a negative supercoil to the DNA molecules during replication, making it essential to the growth of bacteria.⁴ Fluoroquinolones are potent DNA gyrase inhibitors, and they are widely used antibacterial agents in clinics.⁵ However, the fluoroquinolone drugs have encountered the problem of widespread cross-resistance.⁶ Mutations of key residues Ser83 and Asp87 (numbered according to *E. coli* DNA gyrase here

and later unless otherwise specified) in the DNA gyrase A subunit have been identified in many fluoroquinolone-resistant bacterial strains. These mutations significantly reduced the binding affinity of fluoroquinolones to DNA gyrase, which is one of the major mechanisms for the drug resistance.⁷ Gyrase inhibitors different to fluoroquinolones are required for fighting these resistant bacteria.

DNA gyrase is a heterotetrameric enzyme consisting of two A (GyrA) and two B (GyrB) subunits (Fig. 1). While GyrA carries out the DNA cleavage and reunion, GyrB hydrolyzes ATP to introduce negative supercoils to DNA molecules.^{8,9} Both GyrA and GyrB are indispensable for the bioactivity of DNA gyrase in bacteria. Fluoroquinolones target the DNA-cleavage active site on GyrA to efficiently prevent DNA from reunion and release.¹⁰ Other inhibitors have also been reported, but none of them entered the market.¹¹ The ATPase site on GyrB is another attractive site for antibiotic discovery, and drugs targeting GyrB could avoid the fluoroquinolone-resistance caused by GyrA mutations. Novobiocin is a natural product isolated from *Streptomyces* species.¹² It tightly binds to the GyrB ATPase site mainly through hydrogen-bonding (H-bonding) interactions with Asp73 and Arg136 to compete with the adenosine group of the substrate ATP.¹³ In the 1960s, novobiocin was approved

Research Center for Drug Discovery, School of Pharmaceutical Sciences, Sun Yat-Sen University, Guangzhou 510006, China. E-mail: zhuilhao@mail.sysu.edu.cn

† Electronic supplementary information (ESI) available. See DOI: 10.1039/c8md00148k

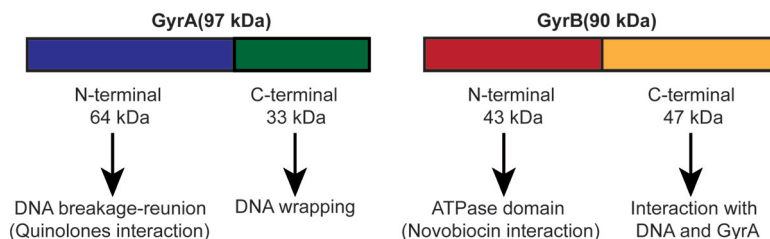


Fig. 1 Domain architecture of A and B subunits of bacterial DNA gyrase from *E. coli*.

for treating the infections of penicillin-resistant *Staphylococcus aureus*, *Streptococcus pneumoniae* and other pathogens. However, it was finally withdrawn by the FDA in 2011 due to its toxicity and low effectiveness.¹⁴ In the recent years, many new GyrB inhibitors have been developed.^{14–16} The inhibitor DS-2969b is currently under clinical development.¹⁶ In addition, two pyrrolamide compounds developed by AstraZeneca were also tested in phase I clinical trials but did not go further.¹⁴ The binding mechanism of these GyrB inhibitors more or less resembles that of novobiocin with overlapping binding sites and similar interacting residues. Therefore, GyrB mutants that are resistant to novobiocin are likely resistant to these inhibitors too. Inhibitors with new scaffolds and novel mechanisms of action are desired to accelerate the discovery of GyrB-targeting antibacterial agents.

Fragment screening is a fast-growing strategy for discovering new drug scaffolds as well as for probing novel druggable sites.^{17–19} In comparison with the traditional high-throughput screening (HTS) approach, which often suffers from extremely low hit rate and thus the need of screening hundreds of thousands of chemicals, fragments are much smaller and enter the binding pockets in the target proteins more easily, and many hits are identified by just screening a few hundred fragments. X-ray crystallographic analysis could reveal the binding modes of these fragment hits in drug targets and also provide the structural basis for fragment growing, merging and linking to exploit new classes of agents. A number of compounds generated by fragment-based lead discovery (FBLD) have entered clinical trials or even reached the market.¹⁹ Fragment screening has also been applied to *S. aureus* GyrB, mainly through computational and NMR-based approaches.^{20–23} These screenings resulted in different initial fragments for lead discovery, and drug-like inhibitors that are more potent than novobiocin were successfully developed.^{20,23} It is worth pointing out that the fragment screening approach often suffers from both high false positives and high false negatives because of the weak affinities and activities of the fragments.^{24,25} More screening efforts are required to identify new fragments for GyrB.

In this study, a library containing 486 rule-of-three (Ro3) fragments was screened against *E. coli* GyrB by combining the protein thermal shift assay (TSA) and ATPase activity assay, resulting in 49 positive hits. Ten cocrystal structures were solved, which revealed three different binding modes of the fragments in the GyrB ATPase domain. Interestingly, one binding mode revealed by two structures disclosed an induced

hydrophobic pocket that has never been identified before. Our structural and biochemical analysis suggested that the ligands binding to this pocket could efficiently block the function of *E. coli* DNA gyrase. The conservation of the pocket and the growing potential of the fragments are also discussed.

2. Results and discussion

2.1 Fragment screening against *E. coli* GyrB

In principle, chemical binding usually stabilizes the target protein and increases its melting temperature (T_m) in the thermal denaturation process. Protein thermal denaturation can be monitored with a dye, which fluoresces only after binding to the hydrophobic surfaces exposed upon protein denaturation.²⁶ In this study, a fluorescence-based thermal shift assay (TSA) was employed to screen a total of 486 fragments to find the potential binding fragments for *EcGyrB_AD*. As the blank control, the T_m of *EcGyrB_AD* without adding any fragments was 55.3 ± 0.2 °C (s.d. from 6 repeats). Considering the general low binding affinities of the fragments, the initial fragment concentration was set to 1 mM. Fragments that could increase the T_m of the protein greater than 0.5 °C (twice of the s.d. of the control samples) were considered as positive hits. Based on this criterion, 33 fragment hits were identified, representing a hit rate of 6.8% (Fig. 2A and Table 1). The T_m changes (ΔT_m) caused by these fragment hits are between 0.5 and 3.1 °C. As expected, the majority of fragments (68.9%) showed no thermal shift (ΔT_m between -0.5 to 0.5 °C), and a number of fragments (24.2%) displayed negative ΔT_m values, which may be due to the nonspecific binding of these fragments to the denatured states of the proteins.²⁷ As a positive control, novobiocin (1 mM) dramatically increased the T_m of *EcGyrB_AD* for about 11.5 °C (Fig. 2B), consistent with its reported strong binding affinity.²⁸

Due to the high false negative in fragment screening, an ATPase activity-based screening strategy was applied in parallel to identify fragment hits from the library. The ATPase domain hydrolyzes ATP to produce the energy for catalysis, and releases ADP and phosphate. When phosphoenolpyruvate, pyruvate kinase, lactate dehydrogenase and NADH are present, the released ADP can be rapidly recycled to ATP. At the same time, NADH will be oxidized to NAD^+ , resulting in a decrease of the absorbance at 340 nm. Therefore, the ATPase activity of GyrB linearly correlates to the absorbance decrease in this coupled system. The inhibitory effect of a fragment can be detected by measuring the percentage change of absorbance

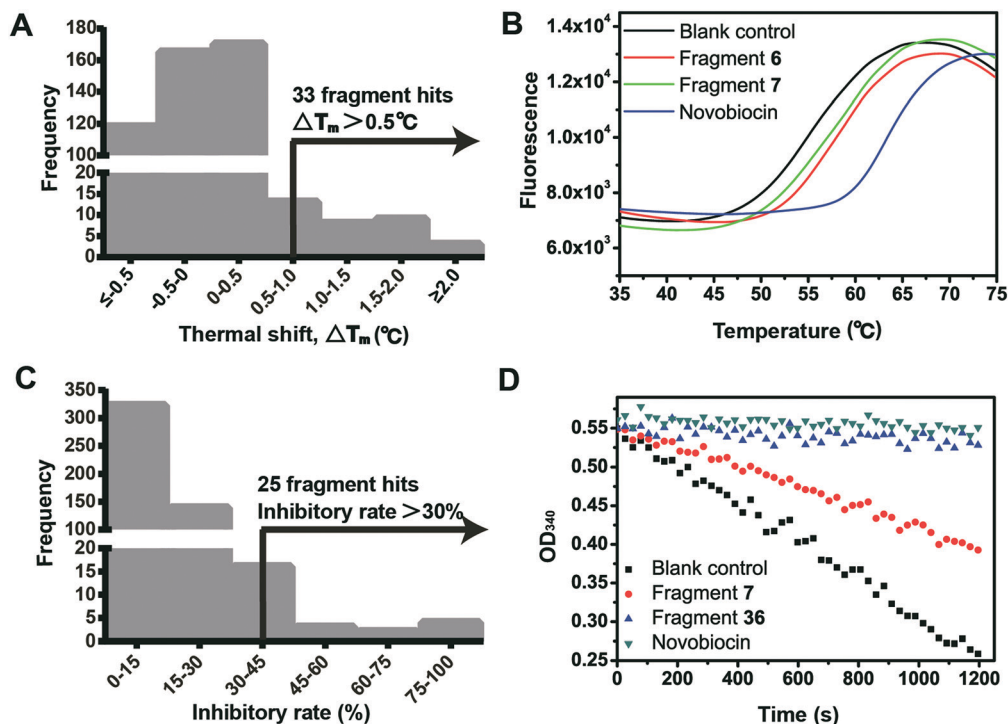


Fig. 2 The fragment screening against *E. coli* DNA gyrase. (A) The fragment screening results from the thermal shift assay (TSA). 33 fragments increased the melting temperature of the *E. coli* DNA gyrase ATPase domain (*EcGyrB_AD*) greater than 0.5 °C, thus were identified as the hits. (B) The representative melting curves of the TSA screening. (C) Histogram of the results of ATPase assay-based fragment screening. 25 fragments showed the inhibitory rate higher than 30% at 1 mM concentration against *E. coli* DNA gyrase, thus were considered as the hits. (D) The representative ATPase assay curves.

Table 1 The summary of fragment screening results

| | No. of compounds | Hit rate ^a (%) |
|---|------------------|---------------------------|
| In-house R03 fragment library | 486 | |
| Thermal shift hits ($\Delta T_m > 0.5$ °C) | 33 | 6.8 |
| ATPase assay hits (inhibitory rate >30%) | 25 | 5.1 |
| Overlapping hits | 9 | |
| Total hits | 49 | 10.1 |
| Binding modes clarified by crystallography | 10 | 2.1 |

^a Hit rate as a percentage of the total fragments screened.

decrease due to the inhibition of ATP hydrolysis. Finally, 25 fragments showed inhibitory rates higher than 30% at 1 mM concentration (Fig. 2C and Table 1). As the positive control, 1 mM of novobiocin totally blocked the ATPase activity of *E. coli* DNA gyrase (Fig. 2D). The IC_{50} values were determined for the fragments with inhibitory rates greater than 60% at 1 mM concentration (Fig. S1A–E[†]). Among these fragments, fragment 49 (4-methylphenylpropionic acid) showed the best inhibitory potency with an IC_{50} value of 0.12 mM and also a good ligand efficiency (LE) of 0.45 kcal mol⁻¹ per heavy atom.

The fragment hits identified by the TSA (33 hits) and ATPase bioassay (25 hits) are partially overlapped (9 hits), resulting in final 49 fragment hits. This relative low overlapping rate between two assays emphasized the neces-

sity of combining independent approaches in fragment screening. The 49 fragment hits are listed in Table S1.[†] Most fragment hits can be grouped into six different scaffolds: benzo-heterocyclic fragments, benzonitrile analogs, phenol fragments, aniline fragments, phenyl-heterocyclic fragments and coumarins (Fig. S2[†]). Besides these six scaffolds, other structures, e.g. the steric adamantane and sulfamide, are also found in the fragment hits. The chemical diversity provides a good opportunity for discovering novel inhibitors. To determine their binding details, 49 fragment hits were used in X-ray crystallography studies.

2.2 X-ray crystallographic analysis of the fragment hits

The X-ray cocrystal structure is important for clarifying the binding mechanism of the fragment hit and guiding the fragment development toward a more potent drug-like molecule, therefore it plays a central role in FBLD. However, crystal soaking often fails to provide enough density for fragment modelling, either due to the block of the fragment binding sites by crystal contacts, or because fragment binding requires protein conformation changes which are not allowed in the crystalline environment.²⁹ To improve the successful rate and to avoid the bias in crystal soaking, four different types of GyrB crystals were soaked (three for *EcGyrB_AD* and one for *SaGyrB_AD*). Finally, cocrystal structures of GyrB_AD with 10 of the 49 fragment hits were determined at

resolutions between 1.45 and 2.74 Å. According to their binding sites and H-bonding patterns, these fragments could be grouped into three classes (Fig. 3A).

Fragments 5, 8, 19, 29, 30, 37 and 45 constitute the first class. These fragments form H-bonding interactions with Asp73, a key residue in coordination of the adenosine group of substrate ATP (Fig. S3A–G†). All these fragments partially overlap with the adenosine group of the ATP analog (ADPNP) and the noviose sugar group of novobiocin when their cocrystal structures are aligned (Fig. S4A†).

In the initial X-ray crystallography trials, only some fragments binding at the site around Asp73 could be identified. To find fragments binding to other sites, fragment 8 was used to saturate the pocket around Asp73, and then the fragments that were able to further increase the protein thermal stability were screened. Using this modified TSA screening method, 6 fragments (1, 6, 9, 24, 25, and 32) were found to further stabilize *EcGyrB_AD* with the $\Delta\Delta T_m$ of 0.7–1.5 °C (Table S2†), suggesting a cooperative binding with fragment 8 at a different site. Interestingly, among these 6 fragments, fragment 24 is similar to the coumarin scaffold of novobiocin, which was shown to mainly interact with two charged residues Arg76 and Arg136.¹³ Fortunately, the X-ray co-structure of *EcGyrB_AD* with fragment 6 (benzofuran-2-carboxylic acid) was finally solved at a resolution of 2.74 Å using the *EcGyrB_AD* crystal. Fragment 6 binds to an alternative site about seven angstroms (Å) away from Asp73. Its carboxyl group makes ionic interactions with the guanidinium group of Arg136 and its furan ring forms a strong cation– π interaction with Arg76, which are similar to the interactions between the coumarin ring of novobiocin and GyrB (Fig. S3H and S4B†). Fragment 6 represents the second class of GyrB-binding fragments we identified (Fig. 3A).

Fragments 7 (4-(4-hydroxyphenyl)sulfanylphenol) and 36 (4-phenoxyphenol) constitute the third class. Both fragments contain a phenol structure, and their phenol moiety forms H-bonds with the carbonyl oxygen of Asp73 and the backbone oxygen of Thr165 (Fig. 3B and C). The other phenol group of

fragment 7 and the phenyl group of fragment 36 were observed to insert into a hydrophobic pocket surrounded by Ile78, Ala91, Ile94, Met95, Val120, Leu132, Ile134, Thr165 and Val167 (Fig. 4B). This pocket is located at the bottom of the ATP adenosine-binding pocket. Interestingly, this hydrophobic pocket is not formed when ADPNP or novobiocin binds to GyrB (Fig. 4A). Binding of fragments 7 and 36 induced the rearrangement of the side chains of Ile78, Met95 and Leu132 and formed this hydrophobic pocket to better accommodate these two fragments (Fig. 4B). Neither substrate ATP nor any published GyrB inhibitors were reported to touch this hydrophobic pocket,^{14,30} indicating a novel inhibition mechanism for fragments 7 and 36 on GyrB.

2.3 Druggability analysis of the new hydrophobic pocket

The new hydrophobic pocket induced by fragments 7 and 36 is close to the binding site of the ATP adenosine group. We further examined the role of such a pocket in regulating the activity of DNA gyrase and in drug development.

At first, the cocrystal structure of the *E. coli* GyrB ATPase domain with fragment 36 was superimposed to that with ADPNP (PDB code 4WUC). Fragments 7 and 36 form an H-bond with Asp73, which is also important for coordinating the adenosine ring of ATP. The phenol group of fragment 36 clashes with the ADPNP adenosine ring, suggesting a direct competition of fragment 36 with the substrate ATP (Fig. 5A). The inhibitory mechanism of fragment 36 was then analyzed by measuring its inhibitory activity of DNA-dependent ATP hydrolysis *in vitro*. The results showed that fragment 36 significantly inhibited the ATP hydrolysis of *E. coli* gyrase in a concentration-dependent manner. However, surprisingly, the apparent K_m of ATP remained unchanged but the V_{max} gradually decreased when the fragment 36 concentration increased, indicating a noncompetitive inhibition mechanism (Fig. 5B). Interestingly, novobiocin and cyclothialidines also showed similar noncompetitive behavior, although the noviose sugar group of novobiocin and the phenol group of cyclothialidines

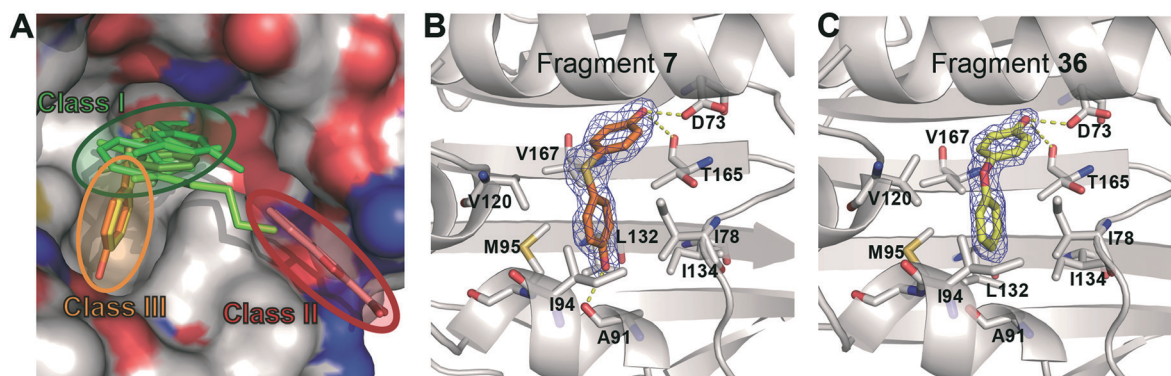


Fig. 3 The X-ray cocrystal structures showing how fragments bind to *E. coli* GyrB. (A) Overlay of the structures of ten fragment hits reveals three different binding modes in the ATPase domain of *E. coli* GyrB. (B and C) Structure basis of fragments 7 and 36 binding to *E. coli* GyrB_AD. The 2Fo–Fc omit electron density maps associated with fragments are shown as blue meshes contoured at 1.0 σ . H-Bonds are shown as yellow dotted lines. All the structural illustrations were prepared with PyMol (<https://pymol.org/>).

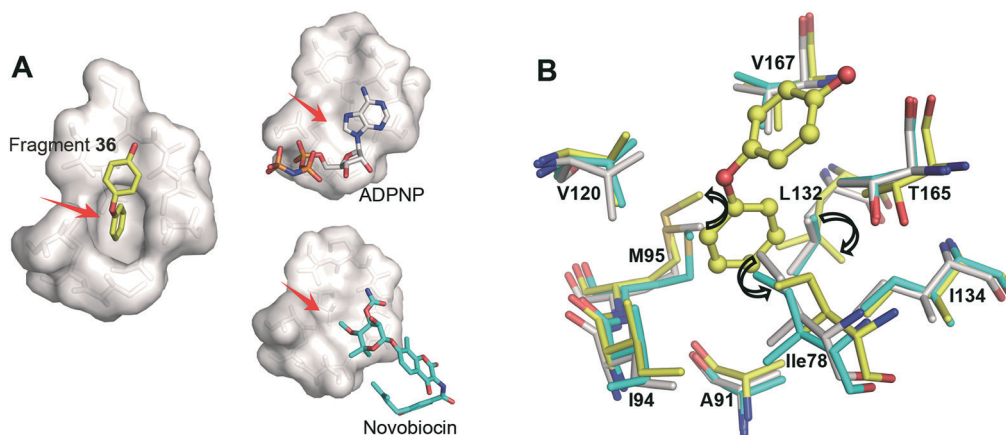


Fig. 4 The hydrophobic pocket is induced upon fragments 7 and 36 binding. (A) The floor of the ADPNP adenosine-binding site of *E. coli* GyrB was drawn as a white surface. When fragment 36 bound, an auxiliary pocket (red arrows) was induced and occupied. When either ADPNP or novobiocin binds, this pocket could not be observed. (B) The side chains of Ile78, Met95 and Leu132 of *E. coli* GyrB undergo the conformation changes as indicated by black arrows in the fragment 36-bound (yellow sticks) state in comparison with the ADPNP- (white) or novobiocin-bound (cyan) states. Fragment 36 is showed as a yellow ball-and-stick model.

clearly overlap with the adenosine ring of ATP according to the high resolution cocrystal structures.^{31,32} Another study suggested that the decreased apparent V_{\max} value only occurred at low substrate ATP concentration (less than 10 mM), and V_{\max} could converge to the same value if ultrahigh concentration of ATP (greater than 1 M) was applied.³³ So far, the results showed that the ATPase inhibitors of GyrB are unlikely to be simple competitive or noncompetitive. We proposed that other factors, such as substrate inhibition, play roles in their action.

The physiological role of DNA gyrase in bacteria is to relax the positive supercoils and to introduce negative supercoils to the double-stranded DNAs during DNA replication. Through an *in vitro* DNA supercoiling activity assay, the topological transition of the relaxed plasmid pHTO-1 to its negatively supercoiled form by recombinant *E. coli* DNA gyrase was measured with or without fragments 7 and 36. In the blank control without chemicals, the DNA gyrase converted nearly half of the relaxed pHTO-1 to the supercoiled form in 30 min. This conversion was blocked completely by fragment

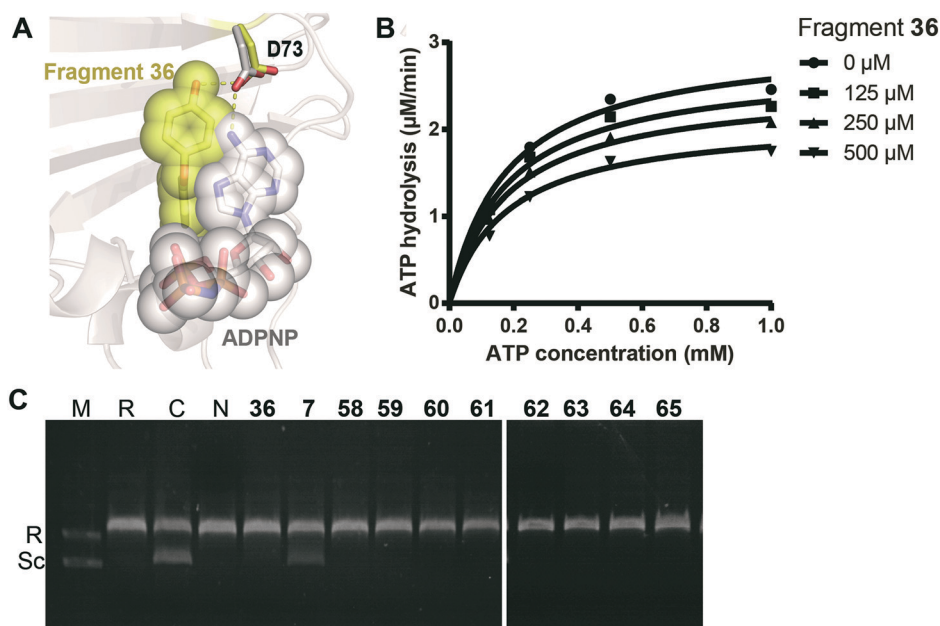


Fig. 5 The inhibitory effects of binding to the induced pocket. (A) Structure superimposition reveals the potential clashes between fragment 36 and ADPNP in the ATPase site of GyrB. (B) *In vitro* DNA-dependent ATP hydrolysis in the presence of different concentrations of fragment 36. (C) Inhibition of DNA gyrase supercoiling activity by novobiocin and the fragments *in vitro*. R, relaxed DNA; Sc, supercoiled DNA; M, DNA maker; C, blank control; N, novobiocin.

Table 2 ATPase inhibitory activities of fragments 7 and 36 analogs

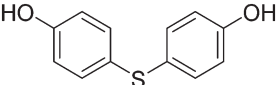
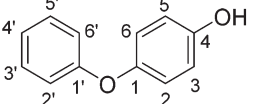
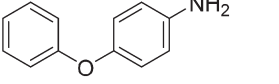
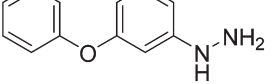
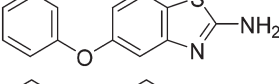
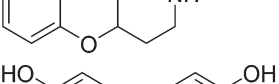
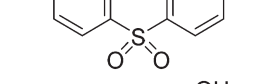
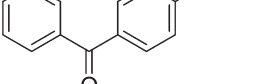
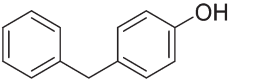
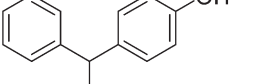
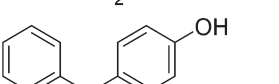
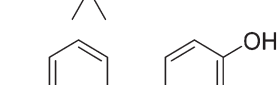
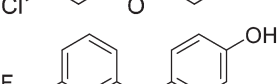
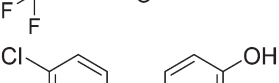
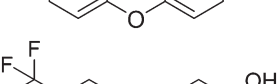
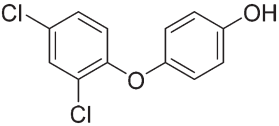
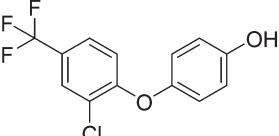
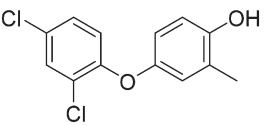
| No. | Structure | ATPase-assay inhibition ^a (%) | IC ₅₀ (mM) | LE (kcal mol ⁻¹ per HA) |
|-----|---|--|-----------------------|------------------------------------|
| 7 |  | 60.2 | 0.95 | 0.28 |
| 36 |  | 96.0 | 0.53 | 0.32 |
| 50 |  | 0 | — | — |
| 51 |  | 0 | — | — |
| 52 |  | 0 | — | — |
| 53 |  | 0 | — | — |
| 54 |  | 0 | — | — |
| 55 |  | 0 | — | — |
| 56 |  | 40.0 | — | — |
| 57 |  | 0 | — | — |
| 58 |  | 96.9 | 0.39 | 0.29 |
| 59 |  | 97.6 | 0.32 | 0.32 |
| 60 |  | 97.6 | 0.24 | 0.28 |
| 61 |  | 97.4 | 0.27 | 0.33 |
| 62 |  | 98.4 | 0.18 | 0.29 |

Table 2 (continued)

| No. | Structure | ATPase-assay inhibition ^a (%) | IC ₅₀ (mM) | LE (kcal mol ⁻¹ per HA) |
|-----|---|--|-----------------------|------------------------------------|
| 63 |  | 99.0 | 0.12 | 0.34 |
| 64 |  | 98.5 | 0.10 | 0.29 |
| 65 |  | 99.5 | 0.084 | 0.33 |

^a Values are measured at 1 mM.

(Fig. 5C). As a positive control, 1 mM novobiocin totally blocked this conversion. These results confirmed that fragments 7 and 36 inhibit not only the ATPase activity but also the DNA topological transition function of DNA gyrase.

Next, the potential of developing fragments 7 and 36 to a potent drug-like chemical was analyzed. The ATPase site of GyrB consists of multiple subpockets. Fragments 7 and 36 occupy the traditional pocket around Asp73 (P1), and also induce and occupy a new subpocket at the bottom of the ATPase site (P3) (Fig. S5[†]). These pockets connect with the ATP-binding pocket (P_{ATP}), coumarin-binding pocket (P2) and a non-touched pocket (P4). Therefore, there is plenty of space for fragment growing, merging and linking in multiple directions to improve the affinities of fragments 7 and 36. Novobiocin and some other GyrB inhibitors suffered from the high lipophilicity-caused strong plasma protein binding and low oral bioavailability.¹⁴ The newly identified pocket is hydrophobic, however, its connection with hydrophilic (sub) pockets, such as the ATP binding pocket (Fig. S5[†]), makes it possible to develop fragments 7 and 36 to drug-like chemicals with appropriate lipophilicity. Furthermore, by binding to the new pocket, inhibitors are likely to overcome the novobiocin-resistant mutations (such as Arg136 mutations) of GyrB.

To further assess the binding capability of the hydrophobic pocket and also identify a better starting point for fragment growing, 14 fragment analogs based on fragments 7 and 36 were screened. Eight fragments (58–65) showed improved ATPase inhibitory activities compared to fragments 7 (IC₅₀ = 0.95 mM) and 36 (IC₅₀ = 0.53 mM) (Table 2 and Fig. S1F–M[†]). The structure–activity relationships (SAR) for these fragments were analyzed. 1) Replacement of Asp73-binding phenol with other H-bond donors (aniline, phenylhydrazine, 2-aminobenzothiazole and piperidine, fragments 50–53) led to the loss of ATPase inhibitory activity at 1 mM. These results indicated that the H-bonding interaction between the phenolic hydroxyl and Asp73 is critical for the inhibitory ac-

tivity, consistent with previous structure observations with fragments 7 and 36. 2) The –SO₂–, –CO– or –CH₂(NH₂)– substitutions (fragments 54, 55, and 57) of the oxygen linker of fragment 36 caused a total loss of ATPase inhibitory activity at 1 mM, and the –CH₂– substitution (fragment 56) partially reduced the inhibitory activity (40.0% inhibition at 1 mM). Interestingly, the addition of two methyl groups to the carbon linker (–C(CH₃)₂–, fragment 58) improved the IC₅₀ to 0.39 mM, suggesting a potential fragment growing direction from the carbon linker. 3) For the phenol/phenyl group that directly interacts with the hydrophobic pocket, adding chlorine and trifluoromethyl improved the inhibitory potency at different levels depending on the positions (fragments 59–62). In particular, double substitutions with chlorine and/or trifluoromethyl at C2' and C4' further improved the IC₅₀ to 0.12 mM (fragment 63) and 0.10 mM (fragment 64), suggesting that the induced pocket prefers larger hydrophobic moieties. The addition of a methyl group at the C3 position further improved fragment 63 to 0.084 mM (fragment 65). These substitutions did not reduce the ligand efficiency of new fragments (Table 2). These fragments with ATPase inhibitory activity (fragments 58–65) were shown to also inhibit the DNA topological transition by gyrase (Fig. 5C).

Finally, the conservation of the new hydrophobic pocket was analyzed. The hydrophobic pocket is located in the center of the ATPase domain. The side chains of the pocket-forming residues all face ATP and are close to its adenosine group. In particular, the side chain of Ile78 forms direct hydrophobic contacts with the ATP adenosine group (PDB code 1EI1). Furthermore, all these residues are also close to the “lid” loop which is essential for the hydrolysis of ATP.³⁴ Thus, the pocket-forming residues are likely important for maintaining the architecture of the ATPase active site. Consistently, the sequence analysis of GyrBs from the major pathogenic bacteria (Fig. S6[†]) revealed that this hydrophobic pocket is highly conserved in the *Proteobacteria* phylum and many other Gram-negative bacteria, and partially conserved

in Gram-positive bacteria, suggesting a broad-spectrum antibacterial potential and a relative lower risk of mutations. Also consistently, the key residue Asp73 is absolutely conserved among all GyrBs analyzed, and the Arg136, which is frequently mutated in novobiocin-resistant *E. coli* and *S. aureus* strains,^{35,36} is not conserved.

3. Conclusion

In this study, by employing TSA- and ATPase inhibition-based screening approaches and X-ray crystallographic analysis, ten fragments with three different binding modes were identified. Among these, fragments 7 and 36 were observed to bind to a hydrophobic pocket which is previously unknown. Our results suggested that the ligands binding in this novel pocket can inhibit the functions of bacterial DNA gyrase. The new hydrophobic pocket and the starting fragments identified in our study provide a novel basis for discovering new GyrB-targeting antibacterial agents.

4. Methods

4.1 Protein expression and purification of *E. coli* and *S. aureus* GyrBs

For the TSA-based fragment screening and crystallographic studies, the 24 kDa fragment of the *E. coli* GyrB (UniProtKB code P0AES6) ATPase domain (*EcGyrB_AD*, residues 15 to 220) was prepared as follows. The DNA coding sequence of *EcGyrB_AD* was inserted into a modified pET20b(+) plasmid (Novagen), and overexpressed as a fusion protein of His₆-sumo-*EcGyrB_AD* using bacterial strain BL21(DE3) (Novagen). The bacteria were grown in 4 liters of Luria-Bertani broth at 37 °C till the OD₆₀₀ = 0.6–0.8, then 0.15 mM of isopropyl-β-D-thiogalactopyranoside (IPTG) was added. The bacteria were further cultured at 18 °C for 20 h for protein expression before being pelleted by centrifugation. The bacterial cells were resuspended with the lysis buffer (50 mM Tris pH 8.0, 400 mM NaCl, and 20 mM imidazole) and lysed by sonication. The cell lysate was centrifuged at 40 000g for 30 min, and the supernatant was loaded onto a pre-equilibrated 5 mL Ni-NTA column (Qiagen). The impurity was washed with 100 mL of the lysis buffer (50 mM Tris pH 8.0, 400 mM NaCl, and 20 mM imidazole). Then, 0.5 mg of Ulp1 enzyme was added onto the column and incubated with the resin at 4 °C overnight to cut off the His₆-sumo fusion partner from *EcGyrB_AD*. The flow-through fraction containing the *EcGyrB_AD* protein was then collected, concentrated, and buffer-exchanged to the equilibrium buffer (20 mM Tris pH 8.0, 70 mM NaCl, and 10 mM β-mercaptoethanol). Then, the protein was loaded onto a 5 ml HiTrap™ Q XL column (GE Healthcare). The column was washed with 25 ml of equilibrium buffer, then the bound proteins were gradually eluted with 175 ml of a linear gradient of NaCl concentration from 70 mM to 1 M. Fractions containing the *EcGyrB_AD* protein were concentrated and buffer-exchanged to the gel filtration buffer (20 mM Tris pH 8.0, 200 mM NaCl, and 10 mM β-mercaptoethanol). The

EcGyrB_AD protein was further purified with the HiLoad 16/60 Superdex 200 pg column (GE Healthcare), and stored at –80 °C in the storage buffer (10 mM Tris pH 8.0, 100 mM NaCl, and 10 mM β-mercaptoethanol). The *S. aureus* GyrB (UniProtKB code P0A0K8) ATPase domain with a loop deletion (*SaGyrB_AD*, residues 14–233, Δ105–126) has been proved to generate high quality crystals.³⁷ The *SaGyrB_AD* was cloned, expressed and purified the same as *EcGyrB_AD*. The protein purities of *EcGyrB_AD* and *SaGyrB_AD* were both above 95% as estimated by SDS-PAGE.

For the ATPase activity-based fragment screening and other enzymatic activity assays, the full-length *E. coli* DNA gyrase was prepared as described.³⁸ In brief, the N-terminal hexahistidine-tagged *EcGyrA* and *EcGyrB* proteins were expressed in BL21(DE3) and purified with a Ni-NTA column separately. Then, two proteins were mixed at a 1 : 1 molar ratio in the gel filtration buffer (20 mM Tris HCl pH 8.0, 200 mM NaCl, and 10 mM β-mercaptoethanol) and incubated on ice for 30 min to allow the self-assembly of the functional A₂B₂ tetramer. The gyrase tetramer was then purified by gel filtration chromatography (HiLoad 16/60 Superdex 200 pg column, GE Healthcare) and stored at –80 °C in the gel filtration buffer before use.

4.2 Fragment screening using the thermal shift assays

To build a concise in-house fragment library, the 2500 fragments from the Ro3 fragment library (Maybridge) were grouped according to their structure similarity, and 486 diverse fragments with molecular weights of 120–280 Da were selected. These fragments follow the ‘rule of three’ criteria and are soluble in aqueous solution (higher than 1 mM). Fragments do not contain any reactive groups, such as quinones and redox cyclers, which might interfere with normal assays and lead to false positive results.

The 486 chemical fragments were screened using a fluorescence-based thermal shift assay (TSA) to look for the hits binding to the ATPase domain of *E. coli* GyrB. Briefly, the 20 μL reactions containing 2 μg of *EcGyrB_AD*, 2× SYPRO orange fluorescence dye (Sigma-Aldrich), 100 mM HEPES pH 7.5, 150 mM NaCl, 1% (v/v) DMSO and 1 mM of each fragments were prepared in the 96-well PCR plates (Life Technologies) on ice. For the blank control, the fragment was omitted from the reaction. For the positive control, novobiocin was used instead of the fragments. The plates were moved to the StepOnePlus Real-Time PCR system (Life Technologies) and incubated at 25 °C for 10 min. Then, the plates were gradually heated from 25 to 95 °C at a rate of 1 °C min⁻¹. The fluorescence intensities of SYPRO orange at 490/530 nm of excitation/emission wavelengths during protein thermal denaturation were recorded every 0.5 min. The melting curves (fluorescence intensities versus temperature) were fitted by a Boltzmann model using Origin 8.0 software (OriginLab) to calculate the protein melting temperature *T*_m. Triplicate assays were applied to all fragments and controls, and the averaged *T*_m was used. The thermal shift (Δ*T*_m) of a

certain fragment was calculated by subtracting the T_m number of the blank control from the T_m of the fragment. A fragment is considered as a hit if its $\Delta T_m > 0.5$ °C.

4.3 Fragment screening using the ATPase inhibition assays

The fragments which could inhibit the ATPase activity of *E. coli* DNA gyrase were also screened from the fragment library. The ATP hydrolysis by DNA gyrase was measured using an assay as described.³⁹ In brief, the ADP production by ATP hydrolysis was coupled with the rapid oxidation of NADH to NAD⁺ and then quantified by measuring the absorbance decrease at 340 nm (ΔA_{340}). For each fragment, a 95 μ L reaction was prepared by mixing 50 mM HEPES, pH 7.5, 150 mM KCl, 8 mM MgCl₂, 5 mM β -mercaptoethanol (Sangon Biotech), 5% DMSO, 250 μ g mL⁻¹ bovine serum albumin, 2 mM phosphoenolpyruvate (BBI Life Science), 160 μ M NADH (BBI Life Science), 5 U of phosphoenolpyruvate (Sigma-Aldrich), 8 U of lactate dehydrogenase (Sigma-Aldrich), 150 nM full-length *E. coli* DNA gyrase, and 1 mM of the fragment in a 96-deepwell plate (Corning) at 30 °C. Then, 5 μ L ATP was added to each well at a final concentration of 0.35 mM to initiate the reactions, and the absorbances at 340 nm were monitored in the first 20 min using the Flex Station 3 (Molecular Devices). The reaction without adding *E. coli* DNA gyrase was used as the baseline, the reaction without adding any fragments was used as the blank control, and the reaction with 1 mM novobiocin was used as the positive control. The inhibitory potency of a fragment against the ATPase activity of *E. coli* DNA gyrase was represented as the inhibitory rate (%), which could be calculated with the equation of the inhibitory rate (%) = [ATPase activity (blank) - ATPase activity (fragment)] / ATPase activity (blank) \times 100% = [ΔA_{340} (blank) - ΔA_{340} (fragment)] / ΔA_{340} (blank) \times 100%. A fragment is considered as a hit if its inhibitory rate is greater than 30% at 1 mM concentration.

4.4 Determining the IC₅₀ against the ATPase activity of *E. coli* DNA gyrase

The ATPase inhibitory rates of the selected fragments at various concentrations were measured as described above. The IC₅₀ value was calculated by fitting the curve of inhibitory rates versus fragment concentrations using the software Prism (GraphPad Software). The logistic dose-response function of activity (%) = 100 / (1 + [I]/IC₅₀)^B was used, where *B* corresponds to the slope factor and [I] corresponds to the inhibitor concentration. The ligand efficiency (LE, kcal mol⁻¹ per heavy atom) of each fragment was calculated using the equation of LE = (1.37/HA) \times pIC₅₀, in which HA is the number of nonhydrogen atoms of the compounds.⁴⁰

4.5 Enzymatic analysis of the inhibitory mode of the selected fragments

The ATP hydrolysis rate (V) of *E. coli* DNA gyrase was measured at different ATP concentrations (125, 250, 500 and 1000 μ M) in the presence of various concentrations of frag-

ment 36. Different nonlinear regressive models (competitive, noncompetitive and uncompetitive) were tried to fit the data using software Prism.

4.6 DNA supercoiling assay

The *E. coli* DNA supercoiling assay was performed using a protocol described previously,³⁸ with slight modification. In brief, for each fragment, a 20 μ L reaction was prepared by mixing 35 mM Tris HCl pH 7.5, 24 mM KCl, 4 mM MgCl₂, 2 mM dithiothreitol, 1 mM ATP, 1.8 mM spermidine, 0.1 mg mL⁻¹ BSA, 6.5% glycerol, 125 ng relaxed pHTO-1 plasmid (TopoGEN), and 1 mM fragment (dissolved at 50 mM in 100% DMSO). The reaction was initiated by adding 25 nM of *E. coli* DNA gyrase, and then incubated at 30 °C for 30 min. The reaction was stopped by adding 5 μ L of 5 \times stop buffer (5% sarkosyl, 0.125% bromophenol blue, and 25% glycerol). The samples were loaded onto a standard 1% agarose gel, and ran at an electric field of 5 V cm⁻¹ for 90 min. The gel was stained with 3 \times 4S Red Plus nucleic acid stain (BBI Life Sciences), and visualized under UV light. Reactions containing 1 mM novobiocin (dissolved at 50 mM in 100% DMSO) or 2% DMSO were used as the positive or blank control, respectively.

4.7 Crystallography

Four different types of crystals were grown using the sitting vapor-diffusion method. 1 μ L protein was mixed with 1 μ L reservoir solution, then the sitting drops were equilibrated against 70 μ L reservoir solution to allow the crystals to grow. Crystals of EcGyrB_AD in the P₂₁2₁2₁ space group were grown at 8 °C with the reservoir solution of 0.1 M Tris-HCl pH 7.5, 2.20 M (NH₄)₂HPO₄, and 10 mM 2-aminobenzimidazole. Crystals of EcGyrB_AD in the P₄₂2₁2 space group as well as in another lattice of the P₂₁2₁2₁ space group were grown in the same drop at 25 °C with the reservoir solution of 0.1 M MES pH 6.0, 2.5 M MgSO₄, and 8 mM tris-(2-carboxyethyl)phosphine (TECP). The crystals of SaGyrB_AD were grown at 25 °C in the solution of 0.1 M Tris-HCl pH 8.0, 0.1 M MgCl₂, and 22% w/v polyethylene glycol 3350. Soaking experiments were done by adding each fragment into the sitting drops at a final concentration of 10 mM and incubating for 30 min to 4 h. The soaked crystals were then immersed in the cryoprotectant solution (the reservoir solution supplemented with 20% glycerol), and flash-frozen in liquid nitrogen for following data collection.

The diffraction data were collected at 100 K at the beamline BL17U1 of Shanghai Synchrotron Radiation Facility (SSRF),⁴¹ and processed using the programs HKL2000 (ref. 42) and XDS.⁴³ The structures were solved by the molecular replacement method using the program Molrep.⁴⁴ The reported structures of *E. coli* and *S. aureus* DNA gyrases (PDB codes 4DUH⁴⁵ and 4P8O⁴⁶) were used as the searching models. Then, iterative adjustments of the structure models were carried out using Coot⁴⁷ and Refmac5.⁴⁸ The fragments were added into the structure models at the late stage of the refinement. The stereochemistry quality of the final structure

models were validated using MolProbity.⁴⁹ The data collection and structure refinement statistics are listed in Table S3.† The coordinates and structure factors of GyrB_AD in the complex with the fragments have been deposited in the PDB under the accession codes 5Z9N (fragment 5), 5Z9M (fragment 6), 5Z4H (fragment 7), 5Z9L (fragment 8), 5Z9P (fragment 19), 5Z9Q (fragment 29), 5Z9F (fragment 30), 5Z4O (fragment 36), 5Z9E (fragment 37), and 5Z9B (fragment 45).

Conflicts of interest

The authors declare no competing financial interests.

Acknowledgements

We thank the staff of BL17U1 beamline at Shanghai Synchrotron Radiation Facility (SSRF), Shanghai, China, for assistance during X-ray diffraction data collection. We thank Professor Xiang-Qun Xie, from the University of Pittsburgh, for his advice in fragment library construction. This research was supported by the National Natural Science Foundation of China (No. 81773636), Guangdong Natural Science Foundation (No. 2017A030313123), and the Program for Guangdong Introducing Innovative and Entrepreneurial Teams (No. 2016ZT06Y337).

References

- 1 C. L. Ventola, *P T*, 2015, **40**, 277–283.
- 2 R. Laxminarayan, A. Duse, C. Wattal, A. K. M. Zaidi, H. F. L. Wertheim, N. Sumpradit, E. Vlieghe, G. L. Hara, I. M. Gould, H. Goossens, C. Greko, A. D. So, M. Bigdeli, G. Tomson, W. Woodhouse, E. Ombaka, A. Q. Peralta, F. N. Qamar, F. Mir, S. Kariuki, Z. A. Bhutta, A. Coates, R. Bergstrom, G. D. Wright, E. D. Brown and O. Cars, *Lancet Infect. Dis.*, 2013, **13**, 1057–1098.
- 3 J. G. Bartlett, D. N. Gilbert and B. Spellberg, *Clin. Infect. Dis.*, 2013, **56**, 1445–1450.
- 4 A. Maxwell, *Biochem. Soc. Trans.*, 1999, **27**, 48–53.
- 5 P. C. Sharma, A. Jain and S. Jain, *Acta Pol. Pharm.*, 2009, **66**, 587–604.
- 6 J. Feliciano, E. Teper, M. Ferrandino, R. J. Macchia, W. Blank, I. Grunberger and I. Colon, *J. Urol.*, 2008, **179**, 952–955, discussion 955.
- 7 K. J. Aldred, R. J. Kerns and N. Osheroff, *Biochemistry*, 2014, **53**, 1565–1574.
- 8 R. J. Reece and A. Maxwell, *Crit. Rev. Biochem. Mol. Biol.*, 1991, **26**, 335–375.
- 9 J. J. Champoux, *Annu. Rev. Biochem.*, 2001, **70**, 369–413.
- 10 F. Collin, S. Karkare and A. Maxwell, *Appl. Microbiol. Biotechnol.*, 2011, **92**, 479–497.
- 11 C. Mayer and Y. L. Janin, *Chem. Rev.*, 2014, **114**, 2313–2342.
- 12 M. Steffensky, A. Muhlenweg, Z. X. Wang, S. M. Li and L. Heide, *Antimicrob. Agents Chemother.*, 2000, **44**, 1214–1222.
- 13 R. J. Lewis, O. M. Singh, C. V. Smith, T. Skarzynski, A. Maxwell, A. J. Wonacott and D. B. Wigley, *EMBO J.*, 1996, **15**, 1412–1420.
- 14 G. S. Bisacchi and J. I. Manchester, *ACS Infect. Dis.*, 2015, **1**, 4–41.
- 15 M. Barancokova, D. Kikelj and J. Ilas, *Future Med. Chem.*, 2018, **10**, 1207–1227.
- 16 T. K. Barman, M. Kumar, T. Mathur, E. Namba, D. Singh, T. Chaira, Y. Kurosaka, M. Yamada, D. J. Upadhyay and N. Masuda, *Antimicrob. Agents Chemother.*, 2018, **62**.
- 17 M. Congreve, G. Chessari, D. Tisi and A. J. Woodhead, *J. Med. Chem.*, 2008, **51**, 3661–3680.
- 18 R. F. Ludlow, M. L. Verdonk, H. K. Saini, I. J. Tickle and H. Jhoti, *Proc. Natl. Acad. Sci. U. S. A.*, 2015, **112**, 15910–15915.
- 19 D. A. Erlanson, S. W. Fesik, R. E. Hubbard, W. Jahnke and H. Jhoti, *Nat. Rev. Drug Discovery*, 2016, **15**, 605–619.
- 20 H. J. Boehm, M. Boehringer, D. Bur, H. Gmuender, W. Huber, W. Klaus, D. Kostrewa, H. Kuehne, T. Luebbbers, N. Meunier-Keller and F. Mueller, *J. Med. Chem.*, 2000, **43**, 2664–2674.
- 21 A. E. Eakin, O. Green, N. Hales, G. K. Walkup, S. Bist, A. Singh, G. Mullen, J. Bryant, K. Embrey, N. Gao, A. Breeze, D. Timms, B. Andrews, M. Uria-Nickelsen, J. Demeritt, J. T. Loch, 3rd, K. Hull, A. Blodgett, R. N. Illingworth, B. Prince, P. A. Boriack-Sjodin, S. Hauck, L. J. MacPherson, H. Ni and B. Sherer, *Antimicrob. Agents Chemother.*, 2012, **56**, 1240–1246.
- 22 M. F. Mesleh, J. B. Cross, J. Zhang, J. Kahmann, O. A. Andersen, J. Barker, R. K. Cheng, B. Felicetti, M. Wood, A. T. Hadfield, C. Scheich, T. I. Moy, Q. Yang, J. Shotwell, K. Nguyen, B. Lippa, R. Dolle and M. D. Ryan, *Bioorg. Med. Chem. Lett.*, 2016, **26**, 1314–1318.
- 23 J. B. Cross, J. Zhang, Q. Y. Yang, M. F. Mesleh, J. A. C. Romero, B. Wang, D. Bevan, K. M. Poutsiaika, F. Epie, T. Moy, A. Daniel, J. Shotwell, B. Chamberlain, N. Carter, O. Andersen, J. Barker, M. D. Ryan, C. A. Metcalf, J. Silverman, K. Nguyen, B. Lippa and R. E. Dolle, *ACS Med. Chem. Lett.*, 2016, **7**, 374–378.
- 24 J. Cramer, J. Schiebel, T. Wulsdorf, K. Grohe, E. E. Najbauer, F. R. Ehrmann, N. Radeva, N. Zitzer, U. Linne, R. Linser, A. Heine and G. Klebe, *Angew. Chem., Int. Ed.*, 2017, **56**, 1908–1913.
- 25 J. Schiebel, N. Radeva, S. G. Krimmer, X. Wang, M. Stieler, F. R. Ehrmann, K. Fu, A. Metz, F. U. Huschmann, M. S. Weiss, U. Mueller, A. Heine and G. Klebe, *ACS Chem. Biol.*, 2016, **11**, 1693–1701.
- 26 F. H. Niesen, H. Berglund and M. Vedadi, *Nat. Protoc.*, 2007, **2**, 2212–2221.
- 27 P. A. McDonnell, J. Yanchunas, J. A. Newitt, L. Tao, S. E. Kiefer, M. Ortega, S. Kut, N. Burford, V. Goldfarb, G. J. Duke, H. Shen, W. Metzler, M. Doyle, Z. Chen, C. Tarby, R. Borzilleri, W. Vaccaro, M. Gottardis, S. Lu, D. Crews, K. Kim, L. Lombardo and D. L. Roussel, *Anal. Biochem.*, 2009, **392**, 59–69.
- 28 G. A. Holdgate, A. Tunnicliffe, W. H. Ward, S. A. Weston, G. Rosenbrock, P. T. Barth, I. W. Taylor, R. A. Pauptit and D. Timms, *Biochemistry*, 1997, **36**, 9663–9673.
- 29 T. G. Davies and I. J. Tickle, *Top. Curr. Chem.*, 2012, **317**, 33–59.

- 30 M. Oblak, M. Kotnik and T. Solmajer, *Curr. Med. Chem.*, 2007, **14**, 2033–2047.
- 31 J. A. Ali, A. P. Jackson, A. J. Howells and A. Maxwell, *Biochemistry*, 1993, **32**, 2717–2724.
- 32 N. Nakada, H. Gmunder, T. Hirata and M. Arisawa, *J. Biol. Chem.*, 1995, **270**, 14286–14291.
- 33 N. A. Gormley, G. Orphanides, A. Meyer, P. M. Cullis and A. Maxwell, *Biochemistry*, 1996, **35**, 5083–5092.
- 34 A. Agrawal, M. Roue, C. Spitzfaden, S. Petrella, A. Aubry, M. Hann, B. Bax and C. Mayer, *Biochem. J.*, 2013, **456**, 263–273.
- 35 M. A. Contreras, *Mol. Microbiol.*, 1992, **6**, 1617–1624.
- 36 M. Stieger, P. Angehrn, B. Wohlgensinger and H. Gmunder, *Antimicrob. Agents Chemother.*, 1996, **40**, 1060–1062.
- 37 G. E. Dale, D. Kostrewa, B. Gsell, M. Stieger and A. D'Arcy, *Acta Crystallogr., Sect. D: Biol. Crystallogr.*, 1999, **55**, 1626–1629.
- 38 L. Li, X. Le, L. Wang, Q. Gu, H. Zhou and J. Xu, *RSC Adv.*, 2015, **5**, 105600–105608.
- 39 M. Rajendram, K. A. Hurley, M. H. Foss, K. M. Thornton, J. T. Moore, J. T. Shaw and D. B. Weibel, *ACS Chem. Biol.*, 2014, **9**, 1312–1319.
- 40 A. L. Hopkins, G. M. Keseru, P. D. Leeson, D. C. Rees and C. H. Reynolds, *Nat. Rev. Drug Discovery*, 2014, **13**, 105–121.
- 41 Q. S. Wang, F. Yu, S. Huang, B. Sun, K. H. Zhang, K. Liu, Z. J. Wang, C. Y. Xu, S. S. Wang, L. F. Yang, Q. Y. Pan, L. Li, H. Zhou, Y. Cui, Q. Xu, T. Earnest and J. H. He, *Nucl. Sci. Tech.*, 2015, **26**, 12–17.
- 42 Z. Otwinowski and W. Minor, *Methods Enzymol.*, 1997, **276**, 307–326.
- 43 W. Kabsch, *Acta Crystallogr., Sect. D: Biol. Crystallogr.*, 2010, **66**, 125–132.
- 44 A. Vagin and A. Teplyakov, *Acta Crystallogr., Sect. D: Biol. Crystallogr.*, 2010, **66**, 22–25.
- 45 M. Brvar, A. Perdih, M. Renko, G. Anderluh, D. Turk and T. Solmajer, *J. Med. Chem.*, 2012, **55**, 6413–6426.
- 46 A. L. Grillot, A. Le Tiran, D. Shannon, E. Krueger, Y. Liao, H. O'Dowd, Q. Tang, S. Ronkin, T. Wang, N. Waal, P. Li, D. Lauffer, E. Sizensky, J. Tanoury, E. Perola, T. H. Grossman, T. Doyle, B. Hanzelka, S. Jones, V. Dixit, N. Ewing, S. Liao, B. Boucher, M. Jacobs, Y. Bennani and P. S. Charifson, *J. Med. Chem.*, 2014, **57**, 8792–8816.
- 47 P. Emsley, B. Lohkamp, W. G. Scott and K. Cowtan, *Acta Crystallogr., Sect. D: Biol. Crystallogr.*, 2010, **66**, 486–501.
- 48 G. N. Murshudov, P. Skubak, A. A. Lebedev, N. S. Pannu, R. A. Steiner, R. A. Nicholls, M. D. Winn, F. Long and A. A. Vagin, *Acta Crystallogr., Sect. D: Biol. Crystallogr.*, 2011, **67**, 355–367.
- 49 V. B. Chen, W. B. Arendall 3rd, J. J. Headd, D. A. Keedy, R. M. Immormino, G. J. Kapral, L. W. Murray, J. S. Richardson and D. C. Richardson, *Acta Crystallogr., Sect. D: Biol. Crystallogr.*, 2010, **66**, 12–21.